Taylor & Francis
Taylor & Francis Group

Phase Transitions
A Multinational Journal

ISSN: (Print) (Online) Journal homepage: www.tandfonline.com/journals/gpht20

Properties of the uniaxial and biaxial nematic phases of the dodecyltrimethylammonium bromide/1-dodecanol/water lyotropic mixture including azo dye and drug molecules

Erol Akpinar, Merve Tabak, Dennys Reis & Antônio Martins Figueiredo Neto

To cite this article: Erol Akpinar, Merve Tabak, Dennys Reis & Antônio Martins Figueiredo Neto (2024) Properties of the uniaxial and biaxial nematic phases of the dodecyltrimethylammonium bromide/1-dodecanol/water lyotropic mixture including azo dye and drug molecules, Phase Transitions, 97:1-2, 66-86, DOI: 10.1080/01411594.2023.2284162

To link to this article: https://doi.org/10.1080/01411594.2023.2284162

PHASE TRANSITIONS
2024, VOL. 97, NOS. 1–2, 66–86
https://doi.org/10.1080/01411594.2023.2284162

Taylor & Francis
Taylor & Francis Group

Properties of the uniaxial and biaxial nematic phases of the dodecyltrimethylammonium bromide/1-dodecanol/water lyotropic mixture including azo dye and drug molecules

Erol Akpinar [a], Merve Tabak[a], Dennys Reis [b] and Antônio Martins Figueiredo Neto [b]

[a]Faculty of Arts and Sciences, Department of Chemistry, Bolu Abant Izzet Baysal University, Bolu, Turkey; [b]Instituto de Fisica, Universidade de São Paulo, São Paulo, Brazil

ABSTRACT

Lyotropic nematic phase properties of novel mixtures of dodecyltrimethylammonium bromide (DTMABr)/1-dodecanol (DDeOH)/water, doping with anionic azo dyes (amaranth and tartrazine) and a drug molecule disodium cromoglycate (cromolyn, DSCG), were investigated. The textures of the uniaxial and biaxial nematic phases were observed by polarizing optical microscopy (POM). Uniaxial-to-biaxial nematic phase transitions were determined from the temperature dependence of the birefringences via laser conoscopy. Partial phase diagrams of the mixtures were constructed as a function of concentrations of dyes and drug molecules by combining the POM and laser conoscopy results. Small-angle X-ray scattering (SAXS) was performed to evaluate micellar structure parameters. The results indicate that those dyes and drug molecules have a greater effect on (a) the nematic-nematic phase transition temperatures, (b) the biaxial-nematic phase-domain range in the partial phase diagrams, and (c) micelle-shape anisotropy, comparing to the addition of other conventional inorganic electrolyte ions. Furthermore, dye and drug molecules may be sequenced in the Hofmeister series of ions, considering the number of ionic groups in their molecular structures and also the chaotropic and/or kosmotropic degrees of the ionic groups. Since these molecules may have a resonance structure (e.g. DSCG), as a result of the existence of the aromatic parts in their structures, this resonance structure should be considered to investigate their effects on the stabilization of the lyotropic nematic phases.

ARTICLE HISTORY
Received 30 August 2023
Accepted 11 November 2023

KEYWORDS
Lyotropic nematic phases; biaxial phase; nematic-nematic phase transitions; surfactant-dye/drug interactions; birefringences; partial phase diagram; polarizing optical microscopy; laser conoscopy

1. Introduction

Lyotropic liquid crystals (LLC) are mesophases that are present in some mixtures, being used in applications related to the fields of biotechnology, such as cosmetics [1], biomedicine [2], drug delivery [3], pharmaceutical [4], creating an environment for biosensors [5], biological membranes [6], food [7], etc., and they have the potential to be used in different fields in the future. Thus, understanding the physicochemical features of the LLCs is crucial for their biotechnological applications. Among LLC structures, nematic phases attracted the attention of the researchers because of the arrangement of the local directors of the micelles along preferred directions in space. These directions are called phase directors or optical axes of the nematic phases. Three types of lyotropic

CONTACT Erol Akpinar akpinar_e@ibu.edu.tr
This article has been corrected with minor changes. These changes do not impact the academic content of the article.
Supplemental data for this article can be accessed online at https://doi.org/10.1080/01411594.2023.2284162.

nematic phases were identified. In the uniaxial discotic (N_D) and calamitic (N_C) nematic phases, the director $\vec{n}$ aligns perpendicular and parallel to an external magnetic field direction, respectively, in the case of the main amphiphile having carbonic chains. There exist two optical axes and three orthogonal two-fold symmetry axes, $\vec{l}$, $\vec{m}$ and $\vec{n}$, where $\vec{n} = \vec{l} \times \vec{m}$ [8–10] in the lyotropic biaxial nematic phase (N_B). Furthermore, the experimental studies proved that, in general, the N_B phase region is located between the two uniaxial nematic phases in the phase diagrams [11–13]. Moreover, the transitions from the N_B phase to the N_D or N_C phases are of second order, as theoretically predicted [14,15].

Some applications of lyotropic nematic phases were reported in the literature. They are used in the production of carbon nanotubes which have applications in the fields of nanoscale electronics [16,17], field-emission sources [18–22], actuators [23], and nanosensors for both biological molecular determination [24,25] and drug release in molecular level [26]. However, some controversies on the stabilization of biaxial nematic phases continue in the literature, mainly, because of the presence of a limited number of mixtures. So, finding and investigating the novel mixtures may help for improvement of the application fields of the lyotropic nematic phases.

In lyotropic mixtures, the main component is the surfactant molecule. In general, strong/weak electrolytes and/or long-chain alcohols (e.g. 1-decanol) can be added to the mixtures. The types of electrolytes and the alkyl-chain length of alcohols determine the properties of the nematic phases. Recently, we reported the lyotropic nematic phase properties of the DTMABr/DDeOH/water ternary mixture by doping with the anionic azo dye Sunset Yellow [27]. That study showed that Sunset Yellow molecule is more effective for obtaining different nematic phases, especially the biaxial one, than conventional inorganic electrolytes (e.g. NaCl, NaBr, etc.). Furthermore, for the first time, we showed that Sunset Yellow molecule has a chaotropic character, and we can place it in the Hofmeister series of ions.

In the present study, we concentrate on preparation of lyotropic mixtures including different dyes (amaranth and tartrazine) and a drug molecule (DSCG) to examine their relative effects on finding different nematic phases via laser conoscopy, polarizing optical microscopy and SAXS. Notice that while the effect of amaranth and tartrazine in dilute micellar solutions was investigated in the literature, but not in lyotropic liquid crystalline state. DSCG was studied in lyotropic chromonic liquid crystals, but not studied in surfactant-based lyotropic liquid crystals yet. All selected molecules present similar partial phase diagrams. However, they affected the nematic-nematic phase transitions and biaxial phase temperature range differently. Furthermore, we classified those molecules in the Hofmeister series of ions by considering the number of ionic groups in their structures. Consequently, the results indicated that dye and drug molecules can also be used to obtain different nematic phases. Considering the surfactant/dye and surfactant/drug interactions in dilute isotropic micellar solutions, it is expected that the results obtained in this study may make contributions to understanding those interactions because both micellar solutions are close-contact with each other.

2. Materials and experimental techniques

DTMABr and DDeOH were available from Sigma and Merck in high purities (>98-99%). Dye molecules Sunset Yellow (dye content: 90%), amaranth (85-95%), tartrazine (dye content: ≥ 85%), and drug molecule disodium cromoglycate, DSCG (≥95%) were also commercially available from Sigma. All dye molecules were purified as described for Sunset Yellow in the literature [27–29]. Briefly, dye molecules were dissolved in a minimum amount of pure water at room temperature, then precipitated by adding absolute ethanol, and finally filtered under vacuum. DSCG was used as received. Ultrapure water was provided by Millipore Direct-Q3 UV system, which produces water having 18.2 MΩ.cm of resistivity at 25°C.

Lyotropic mixtures were prepared by weighing (with 5-digit analytical balance) appropriate amounts of the ingredients into the pyrex test tubes which were closed by their caps and then parafilm to prevent water loss. Then, they were well-homogenized by applying vortex and

centrifuging occasionally. A small amount of water-based ferrofluid was added into the mixtures for well-alignment of the nematic phases in the magnetic field.

Textures of lyotropic nematic phases were characterized under an Eclipse Ci-POL (Nikon, Japan) polarizing optical microscope, attached with a CCD color camera (DFK41AU02, The Imaging Source, Germany) and computer software (NIS-Element-D, Nikon). The temperature stability was provided by Linkam LTS120E heating/cooling stage, which is connected to water circulating bath and Linkam T95-PE heating–cooling controller.

Laser conoscopy is a useful technique (a) to evaluate the two optical birefringences of the nematic phases in an external magnetic field, (b) to unambiguously identify the three nematic phases, and (c) to measure the second-order uniaxial-to-biaxial phase transition temperatures (T_{UB}). The T_{UB} temperatures were determined from the temperature dependence of the birefringences of three nematic phases ($\Delta n = n_2 - n_1$ and $\delta n = n_3 - n_2$, where n_1, n_2 and n_3 are the principal refractive indices of the medium along the 1, 2, and 3 axes of the laboratory frame). In the laser conoscopy set-up, the heat distribution and the temperature stability were provided by, respectively, water circulating bath (Polyscience AD07R, USA) and a temperature controller (Lakeshore 335 with a Pt102 sensor). Because the sample alignment procedure is a key point in the laser conoscopy measurements, the samples were well-aligned in the presence of a magnetic field (~2.2 kG). The sample alignment procedure was previously described in [30,31] and the conoscopic patterns for three nematic phases were similar given in Ref. [31].

Small-angle X-ray scattering (SAXS) was used to estimate the following structural parameters of the nematic phases: average micelles dimensions, uniform thickness of the polar layer, average surfactant aggregation numbers, average number of guest molecules per micelle, average area per polar head and shape anisotropy. The detailed experimental procedure and data analysis are the same of our previous publication [27]. The SAXS measurements were carried out in a Xeuss 2.0 laboratory-based system (Xenocs, France) with a Cu anode microfocus' X-ray source, a FOX3D X-ray mirror, and a pair of Xenocs *scaterless* slits. The monochromatic and collimated incident X-ray beam has a wavelength of 1.5419 Å and square cross section of 0.7 mm side in sample position. The measurements were performed in transmission geometry. The two-dimensional X-ray scattering patterns (Figures S1–S3 of the Supplemental Material) were measured in a Pilatus 300 K detector (Dectris, Switzerland). The sample-to-detector distance was of 937 mm. The samples were transferred into cylindrical Mark-tube capillaries of 1.5 mm diameter (Hilgenberg, Germany), and they were closed with UV-sensitive photopolymer to prevent samples evaporation. For the measurements, a capillary was placed in a temperature-controlled sample holder with precision of ±0.2 °C. Rectangular bars of permanent NdFeB magnets (~1 kG) were attached to the sidewalls of the sample holder to generate a sufficiently homogeneous static magnetic field. From the 2D anisotropic scattering patterns, frame integrations (Figures S4–S6 of the Supplemental Material) were performed along the directions parallel and perpendicular to the magnetic field direction. The frame integrations of 2D SAXS were obtained in circular sectors of 20° around the vertical and horizontal directions of the images (Figure S7 of the Supplemental Material). These operations resulted in curves of X-ray scattering intensity as a function of the momentum transfer modulus, $q = (4\pi/\lambda)\sin\theta$, where 2θ is the scattering angle. The analysis of SAXS data is described in details in the Supplemental Material of [27].

3. Results and discussions

Figure 1 shows the molecular structures of dye and drug molecules: Sunset Yellow, amaranth, tartrazine, and DSCG. Recently, we investigated the uniaxial and biaxial nematic phase properties of lyotropic mixtures including Sunset Yellow in another study [27,32]. The investigation of the nematic phase properties of Sunset Yellow-included mixtures has been repeated in the present study for the comparison with other dye/drug molecules and, within the experimental error limits, similar nematic-nematic phase transition temperatures, temperature-concentration of SSY partial phase diagram, temperature dependence of the birefringences of the nematic phases were obtained.

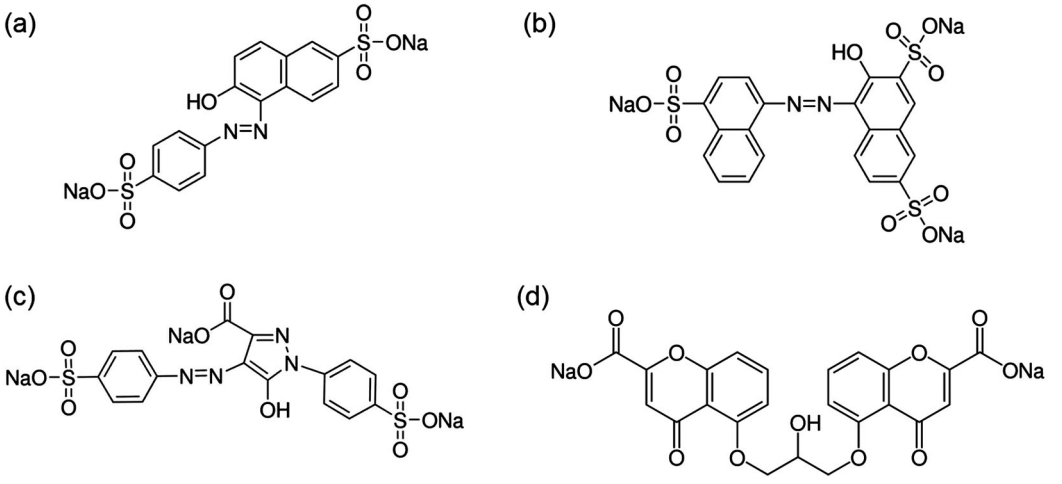

Figure 1. Molecular structures of the molecules: (a) Sunset Yellow, (b) amaranth, (c) tartrazine, and (d) DSCG. Structures of three different dye and drug molecules for comparison. Structures of three different dye and drug molecules for comparison.

The compositions of lyotropic mixtures of DTMABr/DDeOH/water doped with amaranth, tartrazine, and DSCG are given in Table 1, Table 2 and Table 3, respectively, at different dye/drug concentrations. The nematic textures of the mixtures were confirmed by polarizing optical microscopy investigations, with characteristic 'schlieren textures' of nematic phases, and also their homeotropic and planar alignments in the presence of a magnetic field (Figure 2, Figure 3 and Figure 4). Notice that the N_D (N_C and N_B) phase(s) is (are) characterized by homeotropic (planar) alignment. While the N_D phases may be easily distinguished from other nematics, the birefringence measurements by optical conoscopy with compensators or laser conoscopy help to distinguish the N_C phase from the N_B one. The latter was used in the present study to evaluate the second-order uniaxial-to-biaxial nematic phase transitions from the temperature dependence of the birefringences of three nematic phases, and to determine the temperature range of the biaxial nematic phase-domain in the partial phase diagrams.

The birefringences of the three nematic phases, as a function of temperature, for the mixtures given in Table 1, Table 2 and Table 3, were determined from the laser conoscopy. The results are presented in Figure 5, Figure 6 and Figure 7 for each dye/drug molecule.

Table 1. Compositions of the lyotropic mixtures obtained from doping the host mixture with amaranth, in percent molar fractions (X), nematic-nematic phase transition temperatures, and biaxial nematic phase range observed in the partial phase diagram -ΔT_{N_B}.

Mixture	X_{DTMABr}	$X_{amaranth}$	X_{DDeOH}	X_{water}	Phase transitions	$\Delta T_{N_B}/^{\circ}C$
a1	4.985	0.036	1.793	93.186	N_C	–
a2	4.984	0.056	1.793	93.167	N_C	–
a3	4.983	0.066	1.793	93.158	$N_D \xrightarrow{27.2^{\circ}C} N_B \xrightarrow{25.4^{\circ}C} N_C$	1.8
a4	4.983	0.070	1.793	93.154	$N_D \xrightarrow{26.6^{\circ}C} N_B \xrightarrow{24.5^{\circ}C} N_C$	2.1
a5	4.983	0.079	1.792	93.146	$N_D \xrightarrow{23.0^{\circ}C} N_B \xrightarrow{20.7^{\circ}C} N_C$	2.3
a6	4.982	0.088	1.792	93.138	$N_D \xrightarrow{21.4^{\circ}C} N_B \xrightarrow{19.0^{\circ}C} N_C$	2.4
a7	4.982	0.096	1.792	93.130	$N_D \xrightarrow{18.9^{\circ}C} N_B \xrightarrow{15.7^{\circ}C} N_C$	3.2
a8	4.981	0.106	1.792	93.121	$N_D \xrightarrow{16.8^{\circ}C} N_B \xrightarrow{13.7^{\circ}C} N_C$	3.1
a9	4.981	0.114	1.792	93.113	$N_D \xrightarrow{15.2^{\circ}C} N_B$	–
a10	4.980	0.126	1.792	93.102	$N_D \xrightarrow{13.3^{\circ}C} N_B$	–
a11	4.980	0.129	1.792	93.099	$N_D \xrightarrow{13.4^{\circ}C} N_B$	–
a12	4.980	0.141	1.791	93.088	N_D	–
a13	4.979	0.153	1.791	93.077	N_D	–

Table 2. Compositions of the lyotropic mixtures obtained from doping the host mixture with tartrazine, in percent molar fractions (X), nematic-nematic phase transition temperatures, and biaxial nematic phase range observed in the partial phase diagram -ΔT_{N_B}.

Mixture	X_{DTMABr}	$X_{tartrazine}$	X_{DDeOH}	X_{water}	Phase transitions	$\Delta T_{N_B}/^{\circ}C$
t1	4.985	0.036	1.793	93.186	N_C	–
t2	4.984	0.057	1.793	93.166	N_C	–
t3	4.983	0.066	1.793	93.158	N_C	–
t4	4.983	0.070	1.793	93,154	N_C	–
t5	4.983	0.078	1.792	93.147	$N_D \xrightarrow{29.0^{\circ}C} N_B \xrightarrow{28.4^{\circ}C} N_C$	0.6
t6	4.982	0.088	1.792	93.138	$N_D \xrightarrow{27.6^{\circ}C} N_B \xrightarrow{26.8^{\circ}C} N_C$	0.8
t7	4.982	0.095	1.792	93.131	$N_D \xrightarrow{24.9^{\circ}C} N_B \xrightarrow{23.7^{\circ}C} N_C$	1.2
t8	4.981	0.106	1.792	93.121	$N_D \xrightarrow{24.2^{\circ}C} N_B \xrightarrow{22.5^{\circ}C} N_C$	1.7
t9	4.981	0.114	1.792	93.113	$N_D \xrightarrow{22.0^{\circ}C} N_B \xrightarrow{19.9^{\circ}C} N_C$	2.1
t10	4.980	0.130	1.792	93.098	$N_D \xrightarrow{19.2^{\circ}C} N_B \xrightarrow{16.8^{\circ}C} N_C$	2.4
t11	4.980	0.141	1.791	93.088	$N_D \xrightarrow{17.5^{\circ}C} N_B \xrightarrow{14.8^{\circ}C} N_C$	2.7
t12	4.979	0.153	1.791	93.077	$N_D \xrightarrow{15.7^{\circ}C} N_B \xrightarrow{12.6^{\circ}C} N_C$	3.1
t13	4.978	0.165	1.791	93.066	$N_D \xrightarrow{15.2^{\circ}C} N_B$	–
t14	4.978	0.177	1.791	93.054	$N_D \xrightarrow{14.0^{\circ}C} N_B$	–
t15	4.977	0.189	1.790	93.044	N_D	–
t16	4.977	0.200	1.790	93.033	N_D	–
t17	4.976	0.212	1.790	93.022	N_D	–
t18	4.975	0.224	1.790	93.011	N_D	–

Table 3. Compositions of the lyotropic mixtures obtained from doping the host mixture with DSCG, in percent molar fractions (X), nematic-nematic phase transition temperatures, and biaxial nematic phase range observed in the partial phase diagram -ΔT_{N_B}.

Mixture	X_{DTMABr}	X_{DSCG}	X_{DDeOH}	X_{water}	Phase transitions	$\Delta T_{N_B}/^{\circ}C$
d1	4.984	0.053	1.793	93.170	N_C	–
d2	4.983	0.084	1.792	93.141	N_C	–
d3	4.982	0.099	1.792	93.127	$N_D \xrightarrow{24.2^{\circ}C} N_B \xrightarrow{22.9^{\circ}C} N_C$	1.3
d4	4.981	0.105	1.792	93.122	$N_D \xrightarrow{22.9^{\circ}C} N_B \xrightarrow{21.3^{\circ}C} N_C$	1.6
d5	4.981	0.118	1.792	93.109	$N_D \xrightarrow{20.9^{\circ}C} N_B \xrightarrow{18.6^{\circ}C} N_C$	2.3
d6	4.980	0.132	1.791	93.097	$N_D \xrightarrow{18.6^{\circ}C} N_B \xrightarrow{15.8^{\circ}C} N_C$	2.8
d7	4.979	0.143	1.791	93.087	$N_D \xrightarrow{18.0^{\circ}C} N_B \xrightarrow{15.2^{\circ}C} N_C$	2.8
d8	4.979	0.158	1.791	93.072	$N_D \xrightarrow{16.4^{\circ}C} N_B$	–
d9	4.978	0.171	1.791	93.060	$N_D \xrightarrow{15.9^{\circ}C} N_B$	–
d10	4.977	0.189	1.790	93.044	N_D	–

Considering the polarizing optical microscopy investigations and the laser conoscopy results together, the temperature-concentration partial phase diagrams for each guest molecule, i.e. dye and drug molecules, were constructed, Figure 8, Figure 9 and Figure 10. Because it was aimed to compare the effect of each guest molecule on the host mixture DTMABr/DDeOH/water under the same conditions, the phase diagrams were studied in the temperature range of 12.0−30.0°C.

As can be seen from the phase diagram of each of the selected guest molecules, the N_D-N_B and N_B-N_C phase transitions shift to lower temperatures with the addition of guest molecules to the main mixture (D0), which shows only the lyotropic N_C phase, as a function of the temperature. This means that the dyes/drug guest molecules interact with the micelles by acting as electrolytes in lyotropic mixtures [33,34]. In addition, with the increase in the concentration of guest molecules, the N_C phase region narrows in the partial phase diagrams, while the N_D and N_B phase regions expand. This can only be possible if the anionic groups of dyes and drug molecules on the micelle surfaces interact with the cationic head groups of DTMABr surfactant. As it is known, electrolyte ions added to the medium in micellar systems interact with surfactant head groups on the micelle surfaces and change the micelle surface curvature. This change is actually a result of the shielding of the repulsive forces between the surfactant head groups on the micelle surfaces by electrolyte ions.

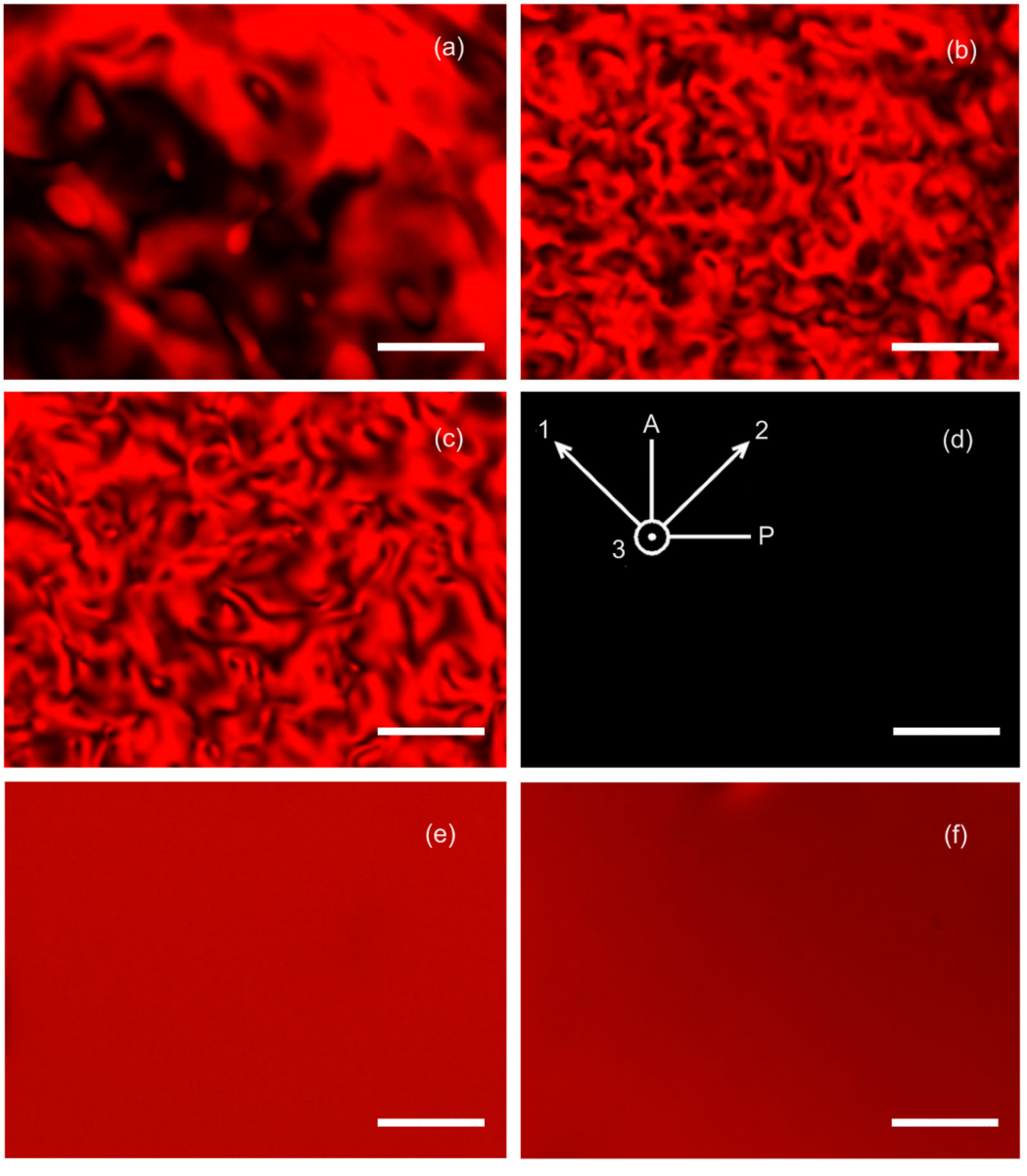

Figure 2. Polarizing optical microscope textures of magnetically non-aligned lyotropic nematic phases for DTMABr/amaranth/DDeOH/water mixture, a6: (a) N_D at 22.0°C, (b) N_B at 20.0°C, and (c) N_C at 15.0°C. After applying the magnetic field of 0.9 kG to those nematic phases at the corresponding temperatures: (d) homeotropic N_D, (e) planar N_B and (f) planar N_C. Objective is 10x and the white bars corresponds to 200 μm. A, P, 1 and 2 given in (d) are the directions of analyzer, polarizer, long capillary axis and magnetic field (only for d, e and f) for all textures, respectively. Similar experimental set-up was applied to tartrazine and DSCG-included mixtures. Lyotropic nematic phase textures of amaranth dye-included sample, observed under polarizing optical microscopy as a function of dye concentration. Lyotropic nematic phase textures of amaranth dye-included sample, observed under polarizing optical microscopy as a function of temperature.

In a study that we recently brought to the literature [32], it was demonstrated that it is possible to obtain different types of nematic phases by controlling the micelle surface curvatures. In that study, it was revealed that the micelle surface curvatures were different in all three nematic phases. In the partial phase diagrams, the least and highest micelle surface curvatures are observed in the N_D and N_C phases, respectively, remaining in the nematic phase region. In the case of micelle surface curvature at moderate levels, the N_B phase is most likely to occur, Figure 11. So, if we go back to the

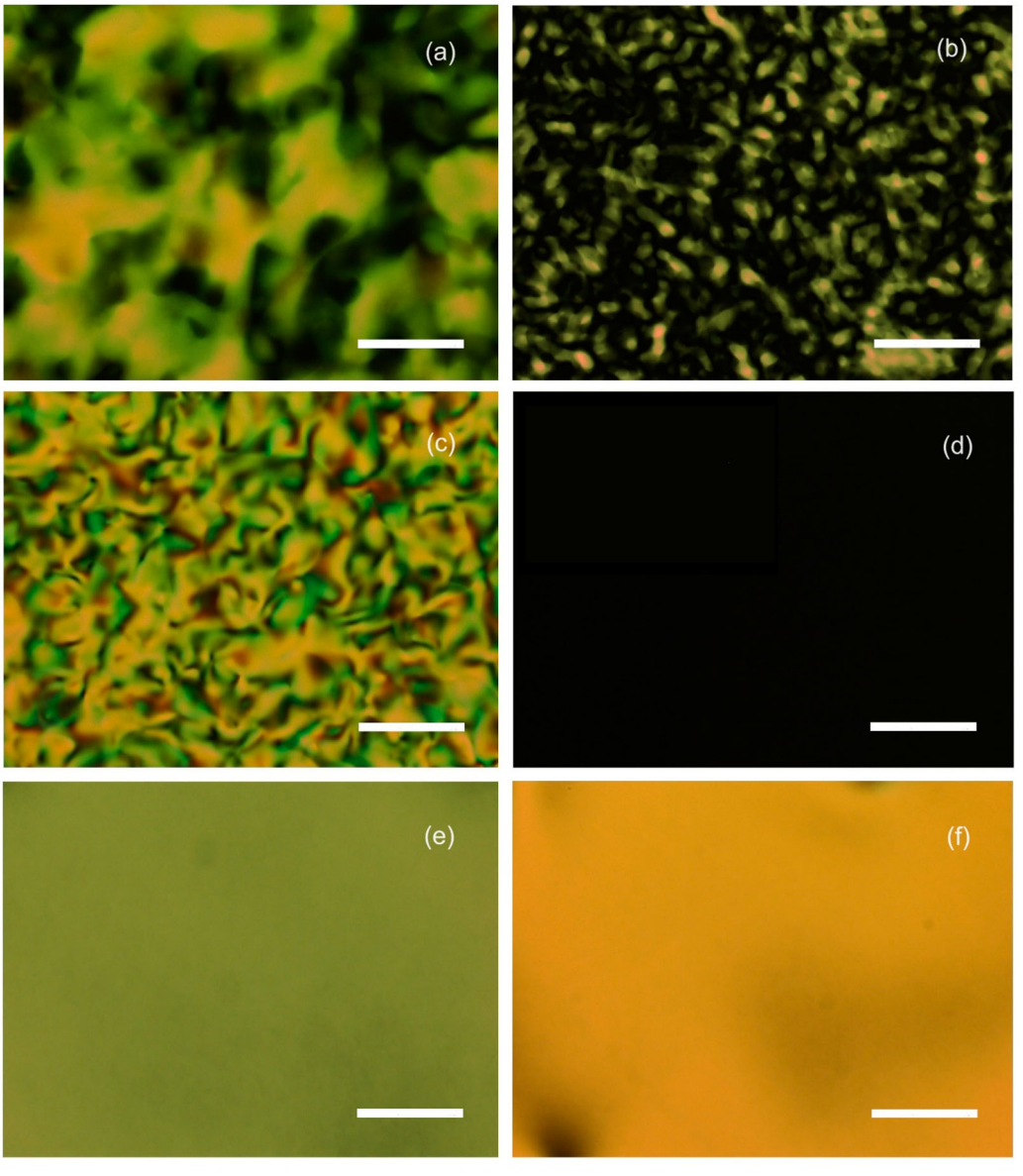

Figure 3. Polarizing optical microscope textures of magnetically non-aligned lyotropic nematic phases for DTMABr/tartrazine/DDeOH/water mixture, t6: (a) N_D at 30.0°C, (b) N_B at 27.3°C, and (c) N_C at 22.0°C. After applying the magnetic field of 0.9 kG to those nematic phases at the corresponding temperatures: (d) homeotropic N_D, (e) planar N_B and (f) planar N_C. Lyotropic nematic phase textures of tartrazine dye-included sample observed under polarizing optical microscopy as a function of temperature.

partial phase diagrams; since guest molecules favor N_D and/or N_B phase formation, they interact effectively with the head groups of DTMABr surfactant molecules on the micelle surfaces and change the micelle surface curvatures.

It is important in the present study to determine which guest molecule is more effective in obtaining different types of nematic phases. Considering the mixtures in Table 1, Table 2 and Table 3 and the mixture with Sunset Yellow (the sample s8 of Ref. [27]), the concentrations of guest molecules in percent mole fractions (X = 0.13) and the total mixture compositions in the

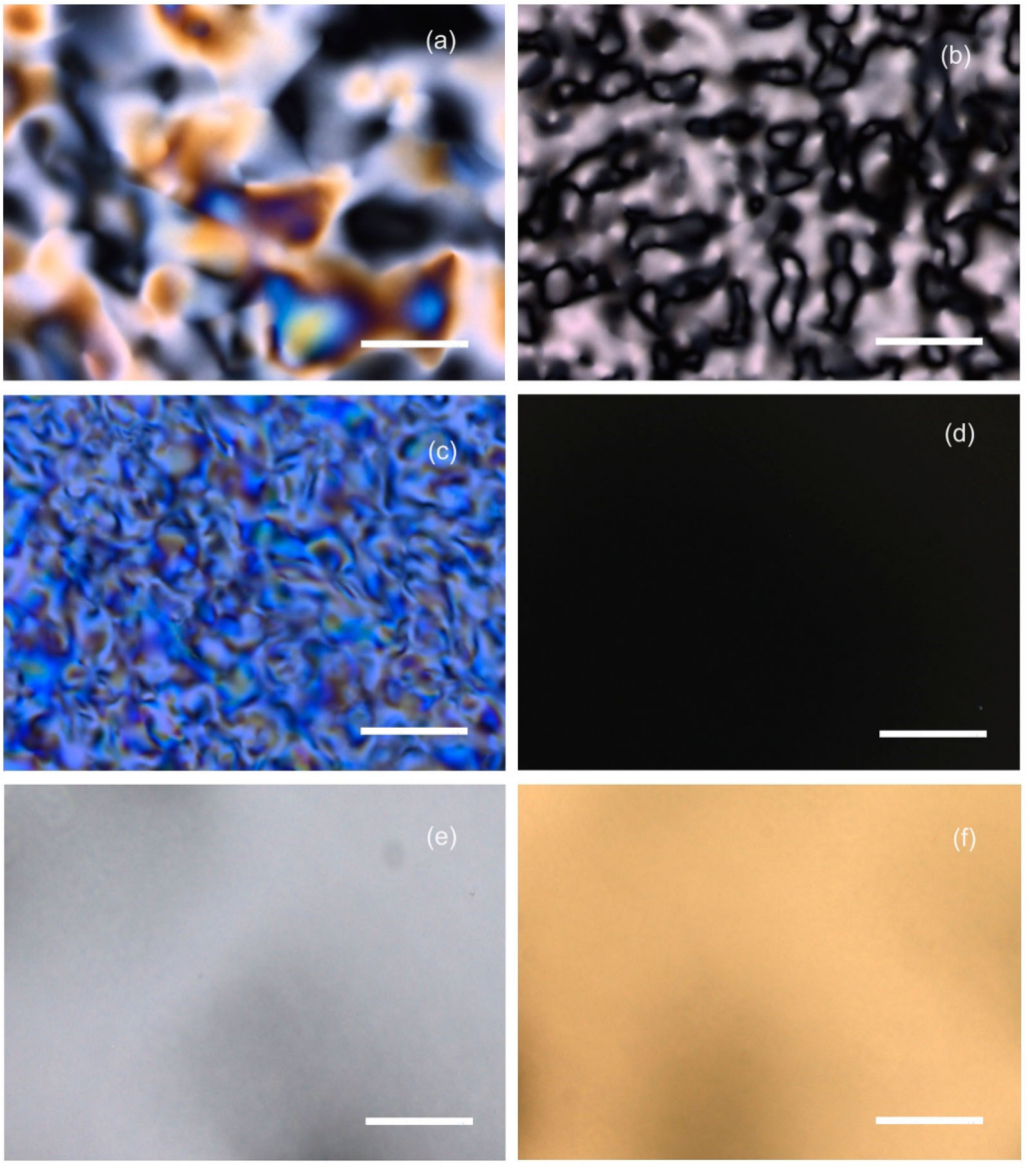

Figure 4. Polarizing optical microscope textures of magnetically non-aligned lyotropic nematic phases for DTMABr/DSCG/DDeOH/water mixture, d6: (a) N_D at 25.0°C, (b) N_B at 17.0°C, and (c) N_C at 14.0°C. After applying the magnetic field of 0.9 kG to those nematic phases at the corresponding temperatures: (d) homeotropic N_D, (e) planar N_B and (f) planar N_C. Lyotropic nematic phase textures of disodium cromoglycate (DSCG) drug-included sample, observed under polarizing optical microscopy as a function of temperature.

mixtures of s8, a11 (amaranth), tartrazine (t10), and d6 (DSCG) are same, within the experimental error limits. Therefore, by comparing the lyotropic nematic liquid crystalline properties of these mixtures, the effects of those molecules and their places in the Hofmeister series can be relatively determined. Among the selected molecules, only Sunset Yellow's place in the Hofmeister series has been determined by us before [27], and there is no information about the others in the literature, to the best of our knowledge. However, before starting a relative comparison, as intended, it would be appropriate to thoroughly examine the molecular structures of the guest molecules given

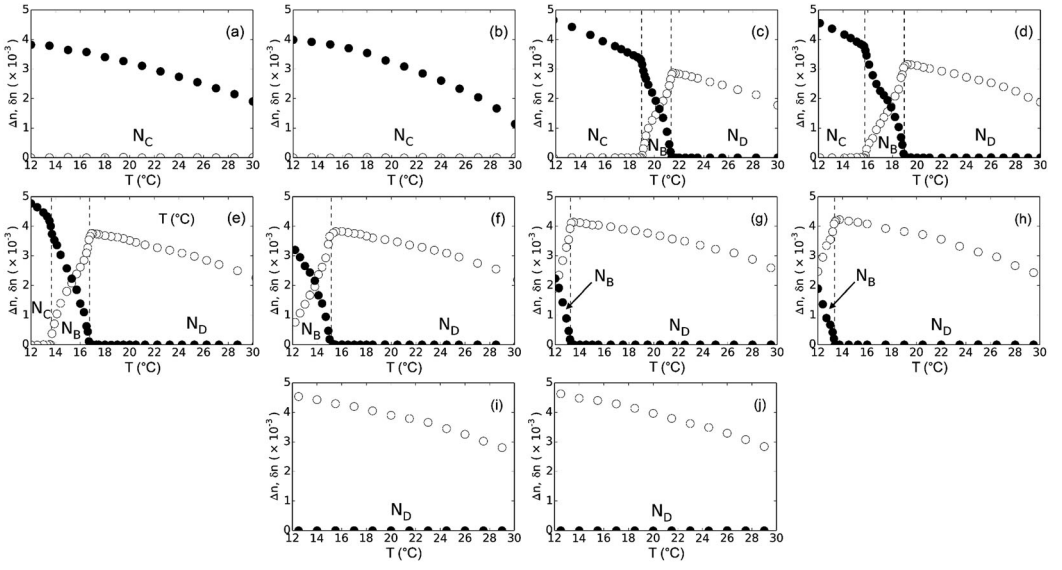

Figure 5. Temperature dependences of the birefringences of the nematic phases for DTMABr/amaranth/DDeOH/water mixtures (Table 1): (a) a1 (b) a2, (c) a6, (d) a7, (e) a8, (f) a9, (g) a10, (h) a11, (i) a12, and (j) a13. Δn (●), δn(○). Birefringences of nematic phases at different temperatures for amaranth dye-included sample. Birefringences of nematic phases at different temperatures for amaranth dye-included sample.

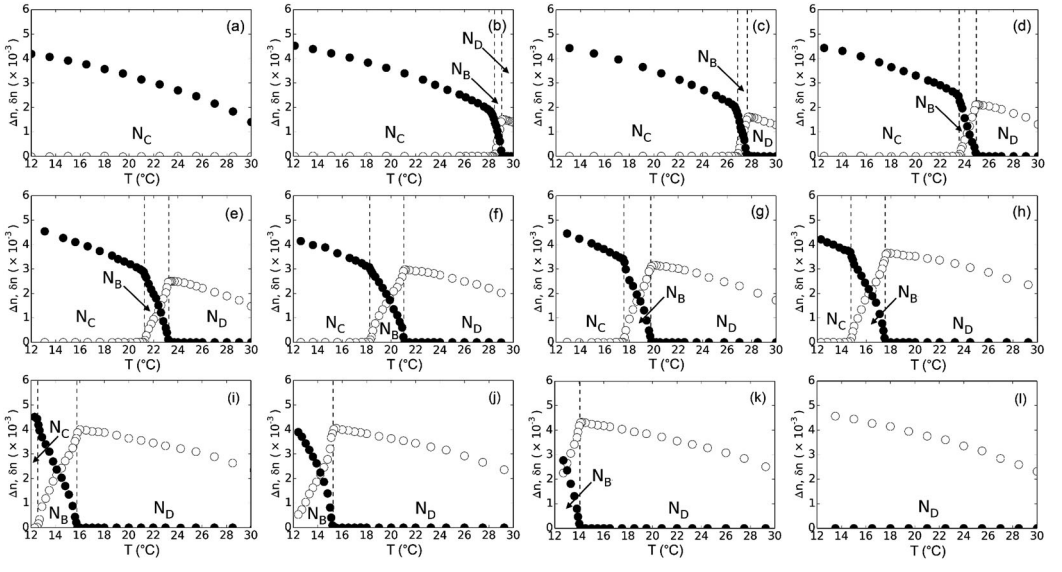

Figure 6. Temperature dependences of the birefringences of the nematic phases for DTMABr/tartrazine/DDeOH/water mixtures (Table 2): (a) t4 (b) t5, (c) t6, (d) t7, (e) t8, (f) t9, (g) t10, (h) t11, (i) t12, (j) t13, (k) t14, and (l) t15. Δn (●), δn(○). Birefringences of nematic phases at different temperatures for tartrazine dye-included sample.

Table 4. Nematic-nematic phase transitions and biaxial nematic phase range determined without considering the number of ions possessed by the molecules at the same dye/drug molecule concentration (X = 0.13).

Mixture	Number of chaotropic $-SO_3^-$	Number of kosmotropic $-COO^-$	$N_D \rightarrow N_B$/°C	$N_B \rightarrow N_C$/°C	ΔT_{NB}/°C
s8*	2	–	21.2	17.1	4.1
a11	3	–	13.4	–	–
t10	2	1	19.2	16.8	2.4
d6	–	2	18.6	15.8	2.8

*From Ref. [27] and confirmed in the present study.

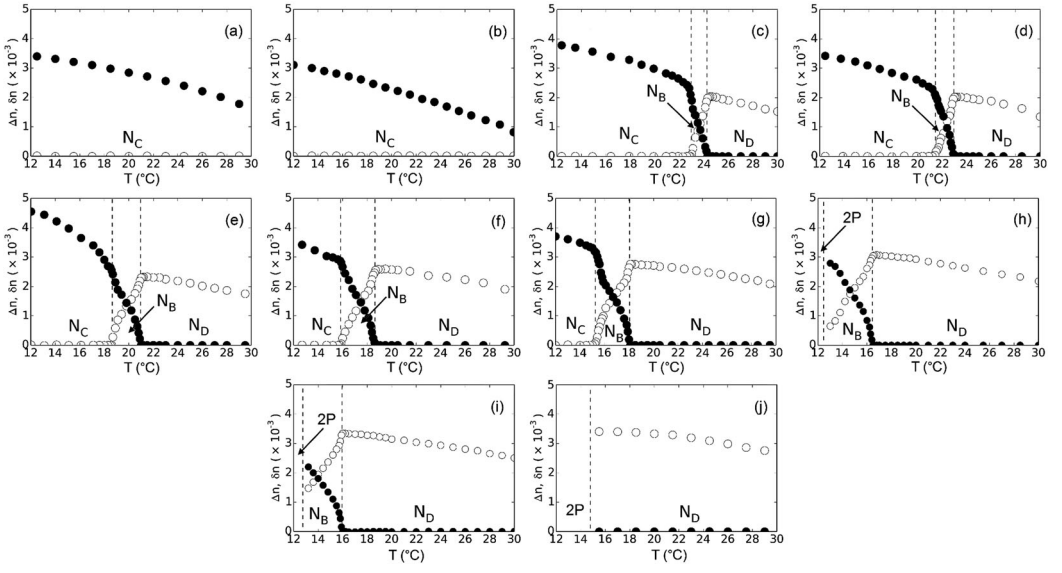

Figure 7. Temperature dependences of the birefringences of the nematic phases for DTMABr/DSCG/DDeOH/water mixtures (Table 3): (a) d1 (b) d2, (c) d3, (d) d4, (e) d5, (f) d6, (g) d7, (h) d8, (i) d9, and (j) d10. Δn (●), δn(○). Birefringences of nematic phases at different temperatures for DSCG drug-included sample.

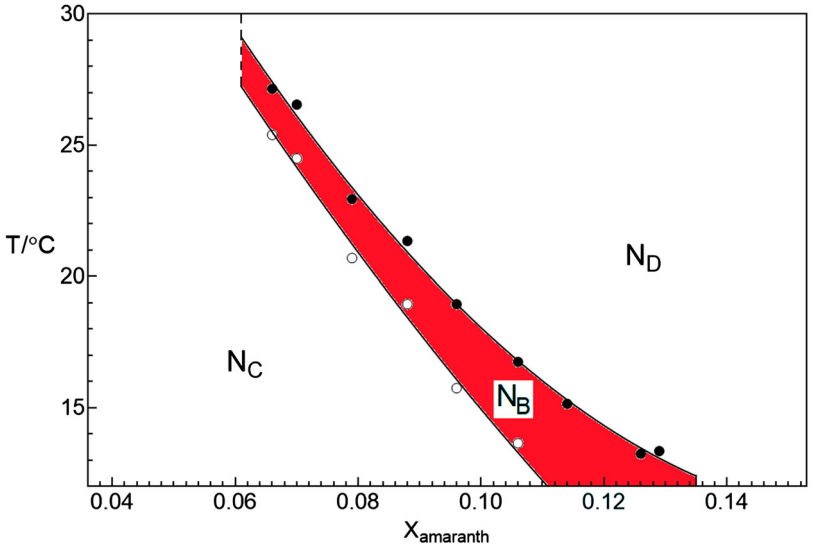

Figure 8. Partial phase diagram of DTMABr/amaranth/DDeOH/water mixtures whose compositions were given in Table 1. Partial phase diagram that shows how the concentration of amaranth dye affects the formation of different nematic phases.

in Figure 1. Sunset Yellow and amaranth have two and three, respectively, chaotropic $-SO_3^-$ anionic groups. While tartrazine has two $-SO_3^-$ and one kosmotropic $-COO^-$, DSCG includes two $-COO^-$. The nematic-nematic phase transition temperatures and biaxial nematic phase region range in the partial phase diagrams given previously for the mixtures in Tables 1–3 and s8, are summarized in Table 4.

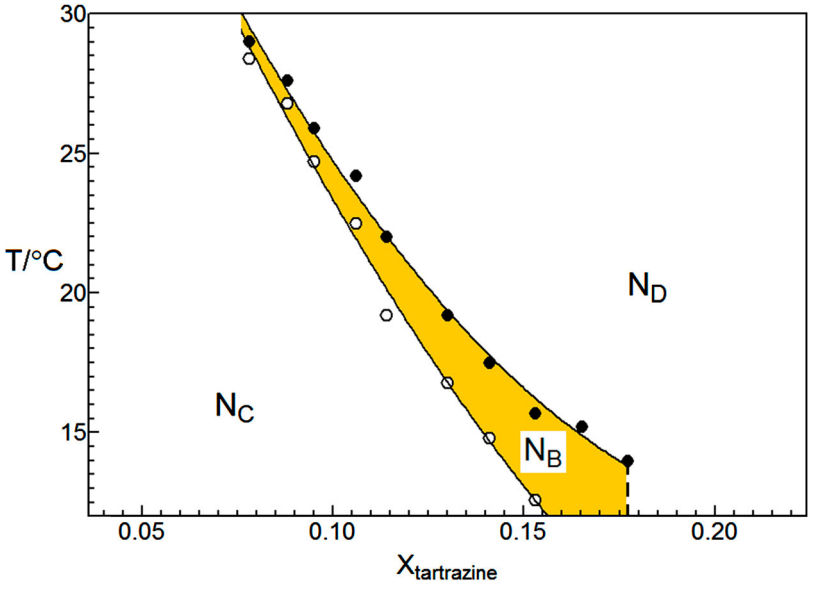

Figure 9. Partial phase diagram of DTMABr/tartrazine/DDeOH/water mixtures whose compositions were given in Table 2. Partial phase diagram that shows how the concentration of tartrazine dye affects the formation of different nematic phases.

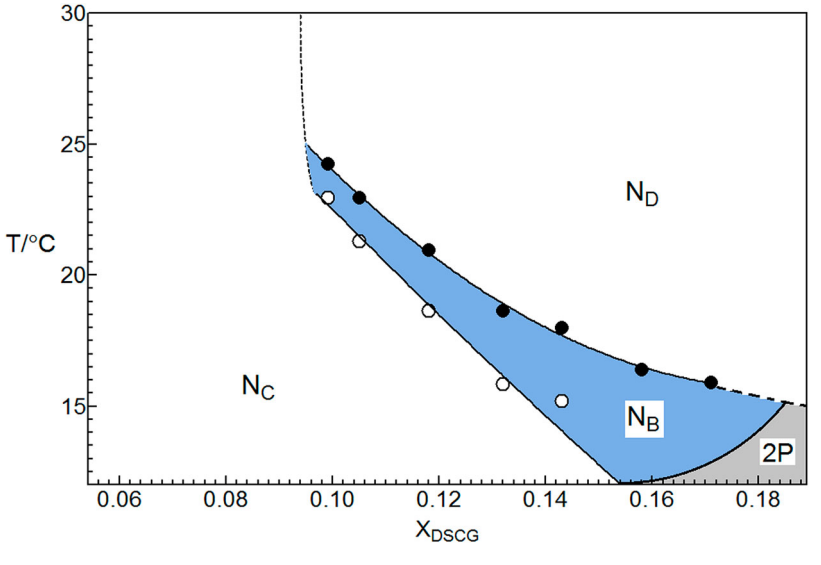

Figure 10. Partial phase diagram of DTMABr/DSCG/DDeOH/water mixtures whose compositions were given in Table 3. 2P: two-phase region. Partial phase diagram that shows how the concentration of DSCG drug affects the formation of different nematic phases.

Before proceeding to the interpretation of the data summarized in Table 4, it would be useful to remind some points. If there are strong chaotropic-chaotropic or kosmotropic-kosmotropic interactions between two ionic species, tightly bound ion pairs are formed [35], resulting in the formation of lyotropic N_D phase. In the opposite case, that is, between two types of ions with quite opposite chaotropic or kosmotropic properties, the interactions are weak and ion pairs weakly bound to each other are formed. This indicates weak chaotropic-kosmotropic interactions and

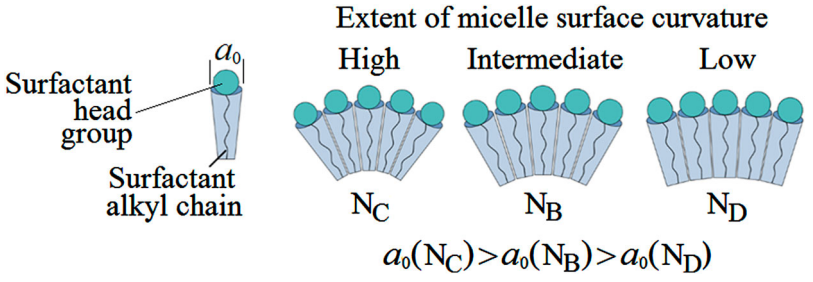

Figure 11. Relationship between the possible extent of micelle surface curvature and the formation of lyotropic nematic phases. a_0: the average area per surfactant head group. The formation of lyotropic nematic phases relates to the extent of micelle surface curvature.

favors the formation of the lyotropic N_C phase. If there are relatively moderate chaotropic-kosmotropic interactions between ionic species, then N_B phases are formed. Comparing the a11 mixture with the t10 mixture, it is seen that, although amaranth and tartrazine molecules with the same mole number contain the same number of ionic groups, the mixture containing amaranth molecule lowered the N_D-N_B phase transition more than tartrazine (about 5.8°C). In other words, in the studied temperature range, the N_D phase region for the a11 mixture was wider in the partial phase diagrams with respect to that for the t10 mixture. In addition, there is no N_C phase region in the mixture a11. This means that the amaranth molecule interacts more strongly with the chaotropic headgroups of DTMABr surfactant molecule [36] on the micelle surfaces than tartrazine. Therefore, in terms of chaotropy, amaranth is more chaotropic than the tartrazine molecule. This is an expected situation because the amaranth molecule interacts with the chaotropic DTMABr surfactant headgroups with three chaotropic ionic groups compared to tartrazine, which has two chaotropic and one kosmotropic groups, and screens the interactions between the headgroups on the micelle surfaces, and then reduces the micelle surface curvature more. As a result, the order of these two molecules in order of increasing chaotropic degree in the Hofmeister series is amaranth > tartrazine.

Similarly, the effects of Sunset Yellow and DSCG molecules, each of which has two ionic groups, can be compared. Here, our expectation was that the mixture containing Sunset Yellow molecule with two chaotropic ionic groups would have a wider N_D region and lower nematic-nematic phase transition temperatures than the mixture containing DSCG with two kosmotropic ionic groups. However, as can be seen in Table 4, the opposite situation was observed in our experimental results. This is only possible with a more comprehensive analysis of the molecular structures of both molecules. In the structure of both molecules (Figure 1), there are two ionic groups and polar OH groups that can partially interact with the head groups on the micelle surfaces [34]. Therefore, from this point of view, the same number of ionic/polar groups are present in the structure of both molecules. The question to be asked at this point is 'although the chaotropic ionic groups of the Sunset

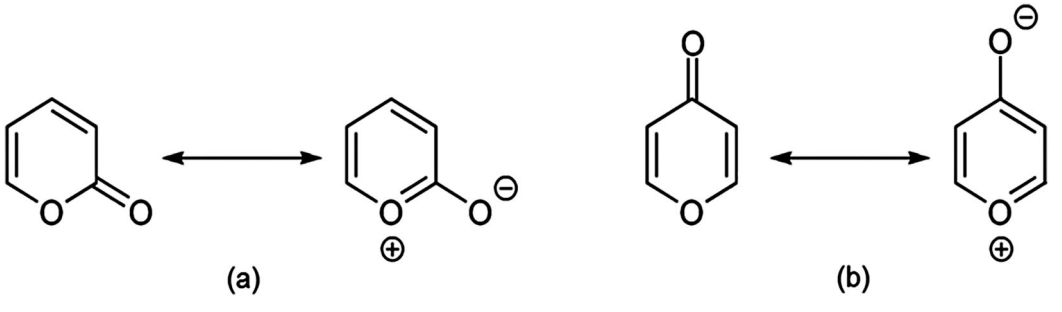

Figure 12. Formation of the resonance structures of (a) pyran-2-one and (b) pyran-4-one [37–39]. Molecules may have different resonance structures.

Yellow molecule interact more strongly with DTMABr head groups than the kosmotropic ionic groups of the DSCG molecule, why does the DSCG molecule (a) reduce the nematic-nematic phase transitions more, (b) favor the formation (expense) of the N_D (N_C) phase, and (c) form tightly bound ion pairs?'. The first aromatic structure to which the carboxylate group is attached in the DSCG molecule is the pyran-4-one structure. In this structure, there is one ether and one ketone groups. It is known that pyran-2-one, which has a similar structure to the pyran-4-one, has a resonance structure as shown in Figure 12 [37]. A similar resonance structure is expected in pyran-4-one, as given in Ref. [38,39], ^{1}H-NMR studies on pyran-4-ones proved the existence of their aromatic nature and resonance structures by observing chemical shifts at 6-8 ppm. Similar chemical shifts in the structure of DSCG were also reported [40]. Thus, the formation of resonance structure for DSCG, yielding two more negative charges in its structure, which can also interact with the positively charged surfactant head groups on the micelle surfaces, is most likely possible. Consequently, according to our results, the molecular structure of DSCG may be in the form of the resonance structure in the micellar solutions, Figure 13, at least, in the lyotropic mixtures studied in the present study.

Positively charged groups in the resonance structure of DSCG molecule will, most likely, interact with the free Br^- ions by the ionization of DTMABr in water or water molecules, while 4 negatively charged ionic groups interact with the head groups of DTMABr. Therefore, it is understandable that such a resonance structure is formed in DSCG molecule and that it remains stable in the presence of positively charged micelles in the solution. As a result, the fact that DSCG seems more chaotropic than Sunset Yellow can only be explained by the formation of a resonance structure of DSCG. Thus, in terms of the chaotropic degree, DSCG > Sunset Yellow. Consequently, considering only the mole fractions of the guest molecules in the mixtures, regardless of the number of ions they contain, the ranking in terms of the degree of chaotropy according to the results given in Table 4 should be as follows.

$$Amaranth > DSCG > Tartrazine > sunset\ yellow$$

Considering the chaotropic properties of Hofmeister series of conventional inorganic anions, the following sequence is valid [41,42]:

$$Br^- < NO_3^- < ClO_3^- < I^- < SCN^- < ClO_4^-$$

In some studies, the relationship between Br^- and NO_3^- is also given as $Br^- \sim NO_3^-$ or $Br^- < NO_3^-$ [43] and this can be attributed to the close chaotropic degrees of both ions. To determine the location of the guest molecules in the Hofmeister series, it would be a more accurate approach to compare them as ions with the same electrical charge, because the electrical charge of the ions to be compared in the Hofmeister series is '−1'. For this reason, a comparison method followed in our previous study will also be applied here [27]. Since the anionic part of the Sunset Yellow molecule has two −1 charged groups, it has a total charge of −2 (S^{2-}). Similarly, amaranth, tartrazine, and DSCG, considering its pyran-4-one structure, have −3 (A^{3-}), −3 (T^{3-}), and −4 (D^{4-}), respectively. As stated earlier, the concentrations of guest molecules in moles or mole fractions are the

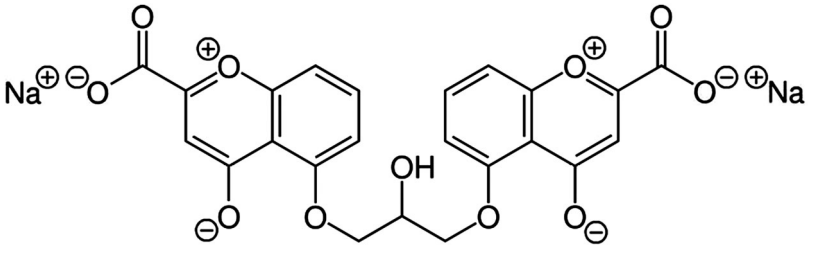

Figure 13. Possible resonance structure of DSCG molecule. Alternative DSCG molecular structure, exhibiting a resonance structure.

Table 5. Considering the number of ionic parts present in the molecular structures of dyes/drug molecules (n_{ion}), nematic-nematic phase transitions and biaxial nematic phase range in the partial phase diagrams.

Ion	n_{ion}	Mixture	X_{guest}	X_{ion}	Observed nematic phase	$N_D \rightarrow N_B$/°C	$N_B \rightarrow N_C$/°C	ΔT_{NB}/°C
S^{2-}	2	s8	0.13	0.26	N_D, N_B, N_C	21.2	17.1	4.1
A^{3-}	3	a6	0.088	0.26	N_D, N_B, N_C	21.4	19.0	2.4
T^{3-}	3	t6	0.088	0.26	N_D, N_B, N_C	27.6	26.8	0.8
D^{4-}	4	d11[a]	0.066	0.26	N_C	–	–	–
Br^-	1	[b]	0.26	0.26	N_D, N_B, N_C	30.1	29.2	0.9
NO_3^-	1	[b]	0.26	0.26	N_D, N_B, N_C	29.2	28.0	1.2
ClO_3^-	1	[b]	0.26	0.26	N_D, N_B, N_C	24.4	22.4	2.0
I^-	1	[b]	0.26	0.26	N_D, N_B, N_C	24.1	21.3	2.8
SCN^-	1	[b]	0.26	0.26	N_D, N_B, N_C	19.3	14.9	4.4
ClO_4^-	1	[b]	0.26	0.26	N_D	–	–	–

[a]The mole fractions of other components (DTMABr, DDeOH, water) are same given in Table 3.
[b]From Ref. [35].

same in the compared mixtures. This means that the same number of guest molecules were added to the host mixture. In the case of the same number of ions, it will be taken as (X_{guest}) x (n_{ion}) = X_{ion} for comparison. Here, since the ionic parts of both the inorganic ions in the Hofmeister series and the dye/drug molecules used in the present study have an electrical charge of −1, the total mole fraction values of the ions (X_{ion}) were calculated from the product of the number of the ion (n_{ion}) and the mole fraction values of the guest molecules added to the host mixture (Table 5). Thus, the presence of the same amount of ionic species as the ions in the Hofmeister series in the mixtures and interacting with the surfactant head groups on the micelle surfaces were ensured. The DTMABr/Sunset Yellow/DDeOH/water mixture (named s8 in this study), which we brought to the literature from our previous studies, was chosen as the starting point for the comparison. In the same study, laser conoscopy measurements of some Hofmeister series ions given above were performed, and nematic-nematic phase transition temperatures and nematic phase types were determined. The results of the aforementioned study and the present study are given together in Table 5 for comparison.

The results given in Table 5 include some information on the chaotropic degree of Sunset Yellow/amaranth/tartrazine/DSCG relative to the inorganic ions in the Hofmeister series. ClO_4^- (D^{4-}) ion gives only N_D (N_C) phase, which means that it has the strongest (weakest) interaction with the DTMABr head groups on the micelle surfaces. Because the SCN^- ion has the lowest nematic-nematic phase transitions and the largest (smallest) N_D (N_C) phase-domain, it follows the ClO_4^- ion in the series. S^{2-} and A^{3-} have very similar N_D-N_B transition, but the N_B-N_C transition for S^{2-} shifts to lower temperature by expensing the N_C phase-domain. So, in terms of chaotropy, $S^{2-} > A^{3-}$. The nematic phase properties of the mixtures with I^-, ClO_3^-, NO_3^-, and Br^- obey the Hofmeister series, i.e. the highly (weakly) chaotropic ion I^- (Br^-) gives nematic-nematic phase transitions at lower (higher) temperatures with larger (larger) N_D (N_C) phase-domain by the increase in the biaxial phase region. According to the phase transition temperatures, T^{3-} should be placed between ClO_3^- and NO_3^-. Thus, the following sequence may be obtained, considering the n_{ion} values of dye/drug molecules:

$$ClO_4^- > SCN^- > Sunset\ Yellow > Amaranth > I^- > ClO_3^- > Tartrazine > NO_3^- > Br^- > DSCG$$

According to the results given in Table 4, i.e. if the n_{ion} values are not considered, the following sequence is assumed

$$ClO_4^- > Amaranth > SCN^- > DSCG > Tartrazine > Sunset\ Yellow > I^- > ClO_3^- > NO_3^- > Br^-$$

However, it seems that the former ordering made by considering the ion numbers of dye/drug molecules, nematic-nematic phase transition temperatures, and the biaxial phase regions in the partial phase diagrams, as in our previous study [27], is more accurate.

Small-angle X-ray Scattering

Small-angle X-ray scattering technique determines the micellar structural parameters and local ordering of the different nematic arrangements. The SAXS patterns of the N_D, N_B, and N_C phases exhibited the characteristic pseudo-lamellar structures and symmetries in the three oriented nematic phases [44,45]. The SAXS curves were analyzed by a simple procedure developed in [27] based on the Intrinsic Biaxial Micelle model, or IBM model [44,45]. This model assumes that in the three nematic phases there are similar orthorhombic micelles stacked in blocks of just a few units in the three directions. Considering the orthorhombic symmetry, as a first order approximation, the micelles are pictured with an average shape of a rectangular parallelepiped [27]. The available volume per micelle, i.e. the volume of a micelle plus a uniform water layer that surrounds it, has the average dimensions A, B, and C, each of which can be evaluated from the SAXS scattered intensity curves. The analysis procedure further assumes the existence of a uniform polar layer around the micelles (i.e. water layer plus electrolytes or other polar dopants plus polar heads of the surfactant and cosurfactant molecules) and the uniform density of the micelles' core (~ 0.80 g/cm^3) composed of alkyl chains of the surfactant and cosurfactant molecules. These hypotheses, together with the A, B, and C average dimensions measured from the SAXS curves, allow the calculation of the micelles core average dimensions A', B', C' and of the uniform thickness of the polar layer, w. From these basic structural parameters, the average aggregation number (N_{agg}), the average area per polar head (a_0), and the average shape anisotropy (SA) of the micelles can be estimated [27]:

$$SA = \left\{ \left[\frac{A' + B'}{2} \right] - C' \right\} / \left[\frac{A' + B'}{2} \right]$$

It enables us to compare the average thickness of the micelles bilayer, C', relative to the average of the other two dimensions, A' and B'. SA gives information on the relative growth of the micelle in the directions perpendicular to the amphiphiles bilayer direction. Another important parameter is the average number of guest molecules (dyes/drug) per micelle, N_{guest}, which is calculated from the ratio of the N_{agg} to the molar ratio between the surfactants and the guest molecules. For the samples s8, a11, t10, d6, a6, and t6, the results of the micelle structural parameters obtained from the SAXS analysis are given in Table 6 and Table 7. Table 8 and Table 9 show the results of the calculations for N_{agg}, a_0, SA and N_{guest}.

Laser conoscopy results exhibited that amaranth, tartrazine, and DSCG molecules bound to the micelles. The micelle bilayer thickness and the average polar layer thickness give us information about the location of the molecules on the micelle surfaces or the penetration to the micelle core. In a recent study [27], the SAXS analysis of DTMABr/DDeOH/water mixture doped with different SSY concentrations and some inorganic electrolytes, separately, showed that the micelle bilayer thickness (C') and the polar layer thickness values were ~29-30 Å and ~14-15 Å,

Table 6. Micelles' average structural parameters obtained from SAXS curves for samples s8, a11, t10 and d6, based on the Intrinsically Biaxial Micelle model and the analysis procedure in [27].

Sample	A (Å)	B (Å)	C (Å)	A´ (Å)	B´ (Å)	C´ (Å)	w (Å)
s8	63.9 ± 1.6	49.9 ± 1.0	43.9 ± 0.2	49.2 ± 2.0	35.3 ± 1.6	29.2 ± 1.3	14.7 ± 1.3
a11	65.1 ± 2.4	49.5 ± 1.1	43.7 ± 0.2	50.3 ± 3.0	34.7 ± 2.2	28.9 ± 1.9	14.8 ± 1.9
t10	64.4 ± 1.9	48.8 ± 0.8	43.7 ± 0.2	49.7 ± 2.3	34.1 ± 1.6	29.1 ± 1.4	14.6 ± 1.4
d6	72.3 ± 3.2	49.0 ± 0.8	43.7 ± 0.2	57.2 ± 3.8	33.9 ± 2.3	28.6 ± 2.1	15.1 ± 2.1

Table 7. Micelles' structural parameters obtained from SAXS curves for samples a6 and t6, based on the Intrinsically Biaxial Micelle model and the analysis procedure in [27]. The data for s8 given in Table 6 are repeated here for comparison.

Sample	A (Å)	B (Å)	C (Å)	A´ (Å)	B´ (Å)	C´ (Å)	w (Å)
s8	63.9 ± 1.6	49.9 ± 1.0	43.9 ± 0.2	49.2 ± 2.0	35.3 ± 1.6	29.2 ± 1.3	14.7 ± 1.3
a6	70.8 ± 2.6	47.8 ± 0.9	44.1 ± 0.2	56.0 ± 3.1	32.9 ± 2.0	29.3 ± 1.8	14.9 ± 1.8
t6	54.2 ± 1.8	47.5 ± 0.9	44.8 ± 0.1	40.3 ± 2.4	33.6 ± 1.8	30.9 ± 1.5	13.9 ± 1.5

Table 8. SA, N_{agg}, a_0 and N_{guest} values for samples s8, a11, t10 and d6.

Sample	SA	N_{agg}	a_0 (Å)	N_{guest}	$N_D \rightarrow N_B$/°C
s8	0.31 ± 0.04	158 ± 5	53 ± 3	3.1 ± 0.1	21.2
a11	0.32 ± 0.05	158 ± 7	53 ± 4	3.0 ± 0.1	13.4
t10	0.31 ± 0.04	154 ± 5	54 ± 3	3.0 ± 0.1	19.2
d6	0.37 ± 0.06	174 ± 8	52 ± 5	3.4 ± 0.2	18.6

respectively, for SSY and electrolytes. It is well-known that electrolyte ions are present in the polar layer at the micelles' surfaces and cannot penetrate to the micelle core. Thus, obtaining similar C' and w values for electrolyte ions and SSY proved that the plank-like SSY molecules do not penetrate inside the core of the micelles. Instead, they localize on the micelles' surface or in the water layer region with their largest surface being parallel or at most inclined to the micelles' surfaces. Remember that we used the same DTMABr/DDeOH/water host mixture with the same mole fractions of each component given in the reference [27]. Because the similar C' and w values are obtained in the present study, Table 6 and Table 7, the guest molecules amaranth, tartrazine, and DSCG have to be localized on the micelle surfaces like SSY molecules, i.e. they do not penetrate inside the micelle core and localize on the micelle surfaces with their largest molecular surfaces.

The average area per polar head (a_0) gives information on the interactions between the ionic species at the micelle surfaces. If the ions interact strongly or weakly with the surfactant head groups, they screen the repulsions between the surfactant heads groups and the a_0 values of the surfactants decrease. The strong (weak) interactions give rise to the formation of the close-contact (loosely bound) ion pairs. From the Hofmiester series point of view, while surfactant head groups and ions with similar chaotropic or kosmotropic character leads to formation of close-contact ion pairs, those with opposite character form loosely bound ones. In Table 8 and Table 9, the a_0 values are given. Considering the charges of both the head group of DTMABr and the ionic parts of each guest molecules, they behave as 1:1 electrolyte on the micelle surfaces and the head group of one DTMABr molecule interacts with only one ionic part of each guest molecule. So, in our case, it can be assumed that the a_0 is a measure of the strength of the interaction between surfactant head group and the guest molecule per its ionic part. SSY and amaranth have two and three same chaotropic ($-SO_3^-$) groups, and each $-SO_3^-$ group causes the same value of the a_0 for s8, a11 and a6 (53 Å). When one of the $-SO_3^-$ group in the structure of the amaranth is replaced by one kosmotropic $-COO^-$, i.e. tartrazine molecule, it is expected that the average chaotropy per ionic part slightly decreases with respect to the amaranth molecule, and the interactions between DTMABr head group and tartrazine is slightly weaker than DTMABr head group and amaranth. The last situation is confirmed with the a_0 values for t10 (54 Å) and t6 (56 Å). DSCG molecule has two kosmotropic–COO^- groups. In the literature, there is no information about chaotropic or kosmotropic character of the additional ionic parts in the aromatic part of DSCG molecule

Table 9. SA, N_{agg}, a_0 and N_{guest} values for samples a6 and t6. The data for s8 given in Table 8 are repeated here for comparison.

Sample	SA	N_{agg}	a_0 (Å)	N_{guest}	$N_D \rightarrow N_B$/°C
s8	0.31 ± 0.04	158 ± 5	53 ± 3	3.1 ± 0.1	21.2
a6	0.34 ± 0.05	169 ± 7	53 ± 4	2.2 ± 0.1	21.4
t6	0.16 ± 0.05	130 ± 5	56 ± 4	1.7 ± 0.1	27.6

(Figure 13). So, it is not easy to interpret its a_0 value if the X_{ion} (the total mole fraction values of the ions) values are not considered. However, as we discussed in the results of the laser conoscopy, the average degree of the kosmotropic/chaotropic character of DSCG as a molecule is between SSY and tartrazine if we take into account the transition from discotic nematic phase to the biaxial nematic phase. From this respect, it can be said that the SAXS results are in good agreement with both laser conoscopy and polarizing optical microscopy.

Among the micelle structural parameters obtained from the SAXS analysis, considering by the X_{ion} values, the N_{guest} values (Table 9) are more appropriate. By this way, all results obtained from laser conoscopy, polarizing optical microscopy and SAXS measurements are significant. As it can be seen in Table 9 (remember that s8, a6, t6 and d11 introduce same mole number of ionic parts to the mixtures with $X_{ion} = 0.26$), as the kosmotropic character of the ionic parts of the guest molecules increases, the N_{guest} values decrease by favoring (unfavoring) the formation of N_C (N_D) phase. Although it cannot be possible to calculate the N_{guest} value for DSCG-included mixture (d11), because it gives only N_C phase, experimental results in the literature showed that the highest micelle surface curvature is observed in the N_C phase compared with the other nematic phases, which indicates the higher a_0 values. So, DSCG has to exhibit the highest (smallest) a_0 (N_{guest}) values with respect to the other guest molecules. Consequently, the increasing order of chaotropic character of the guest molecules in the Hofmeister series by considering the ion numbers in the structure of dye/drug molecules is SSY > Amaranth > Tartrazine > DSCG. This order is in good agreement with the laser conoscopy results and the literature [27]:

$$ClO_4^- > SCN^- > Sunset\ Yellow > Amaranth > I^- > ClO_3^- > Tartrazine > NO_3^- > Br^- > DSCG$$

As a result, the chaotropic degrees of the dyes and drug molecules were determined by considering the Hofmeister series of ions. It is also seen from the results of the present study that surfactant-based lyotropic nematic phases can be obtained by using dye and/or drug molecules containing ionic groups in addition to traditional inorganic electrolyte ions. Another important point is that different types of nematic phases can be obtained by using less amount of dye/drug molecules compared to electrolytes containing inorganic ions, and it is possible to control for obtaining a larger biaxial nematic phase region in partial phase diagrams. Because this is an active research field, the results obtained from the present study have contributed significantly to the studies in this field.

Furthermore, a comparison of the structural parameters for samples of same compositions but different concentrations of the guest molecules is done in the following. Figure 14 shows the data for the micelles core dimensions for amaranth and tartrazine samples as functions of the number of guest molecules per micelle (N_{guest}), from Table 6 and Table 7. It is clearly seen that while B' and C' are almost constant with the increase of dye concentration for both dyes, the A' dimension increases with the concentration of tartrazine while it decreases with amaranth concentration. A' is a dimension perpendicular to the amphiphilic bilayer dimension C'. It means that the increase of tartrazine concentration induced a growth of the micelle perpendicularly to the amphiphilic bilayer, while the increase of amaranth concentration induced a reduction of the micelle in this same dimension. These can also be seen in the shape anisotropy and aggregation number as functions of N_{guest} for these same samples, in Figure 15. The increase of A' for amaranth samples reflects in the increase of SA and N_{agg} with a higher concentration of the dye, while the opposite is true for tartrazine samples. The average area per polar head, a_0, decreases a bit with tartrazine concentration while it doesn't change significantly for amaranth samples. From which it is concluded that the growth or degrowth of the micelles are due to an increase or decrease of the average number of amphiphilic molecules in the micelles, and not due to an increase or decrease in the packing of the amphiphiles. This is the kind of growth or degrowth promoted by the increase of dyes concentrations.

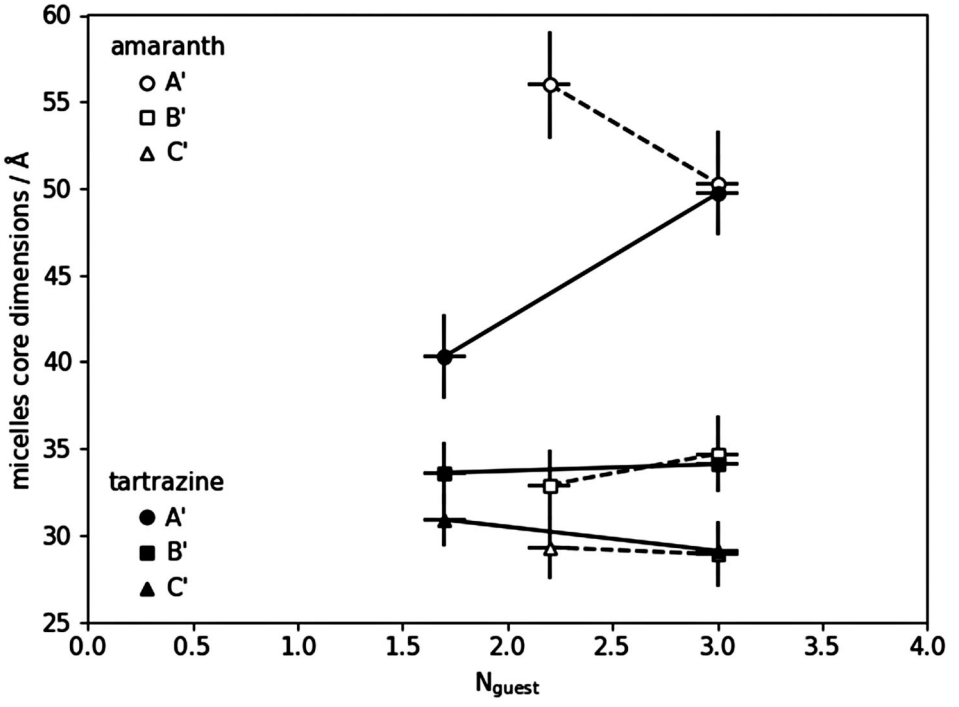

Figure 14. Micelles core average dimensions A′, B′, C′ as functions of the number of guest molecules per micelle (N_{guest}), for tartrazine samples t6 and t10, and for amaranth samples a6 and a11, according to Tables 6 and 7. Change in micelles core average dimensions as functions of the number of guest molecules per micelle for dye molecules.

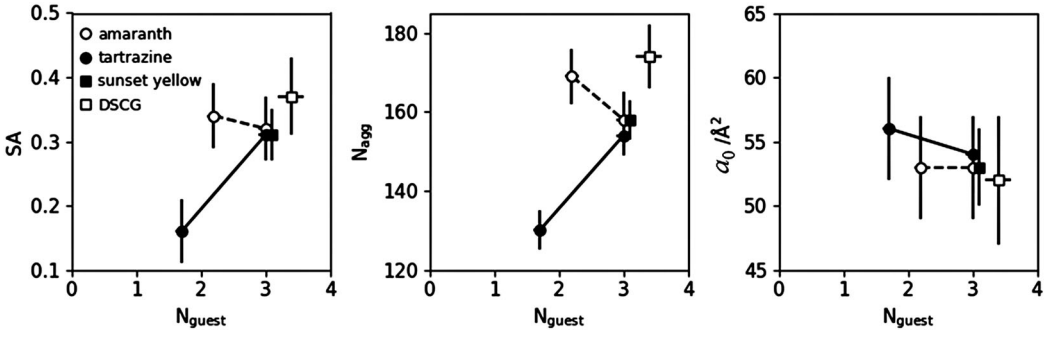

Figure 15. Shape anisotropy (SA), average aggregation number (N_{agg}), and average area per polar head (a_0) for the micelles as functions of the number of guest molecules per micelle (N_{guest}), according to Tables 8 and 9. Some micellar parameters for nematic phases depending on the number of dye/drug molecules per micelle.

4. Conclusions

In the present study, it was aimed to investigate the effects of interactions between ionic species on the micelle surfaces in the formation of lyotropic nematic phases by using cationic surfactant DTMABr and dye/drug guest molecules containing anionic groups in their molecular structures. The point of attention in these guest molecules is the number of ionic groups in their molecular structures and also the chaotropic and/or kosmotropic degrees of the ionic

groups because these properties are an important parameter in the interactions of surfactant molecules and dye/drug molecules. The results indicate that those guest molecules have a greater effect on (a) the nematic-nematic phase transitions, (b) the biaxial nematic phase-domain range in the partial phase diagrams, and (c), because higher birefringences mean higher micelle-shape anisotropy, micelle-shape anisotropy, than the conventional inorganic electrolyte ions. Furthermore, dye/drug molecules containing ionic parts in their structures may be sequenced in the Hofmeister series of ions. However, it would be pointed out that since the dye/drug molecules may have a resonance structure as a result of the existence of the aromatic parts in their structure, this resonance structure should be considered to investigate their effects on the formation of the lyotropic nematic phases. This may be also an important point for lyotropic chromonic liquid crystals (LCLCs) because the drug molecule DSCG has been widely investigated to form LCLCs.

Acknowledgements

Erol Akpinar (EA) and Antonio M. F. Neto (AMFN) designed the experimental parts of the studies, then analyzed and discussed the results. EA and Merve Tabak performed the experimental work. SAXS data analysis and discussions were performed by AMFN and Dennys Reis.

Disclosure statement

No potential conflict of interest was reported by the author(s).

Funding

This work was supported by Bolu Abant Izzet Baysal University Directorate of Research Projects: [Grant Number 2022.03.03.1555]; The National Council for Scientific and Technological Development (CNPq): [Grant Number 465259/2014-6]; The São Paulo Research Foundation (FAPESP: [Grant Number 2014/50983-3; 2016/24531-3]; The Scientific and Technological Research Council of Turkey (TÜBİTAK): [Grant Number 120Z721].

ORCID

Erol Akpinar http://orcid.org/0000-0002-9854-5177
Dennys Reis http://orcid.org/0000-0002-2422-2260
Antônio Martins Figueiredo Neto http://orcid.org/0000-0002-6339-8699

References

[1] Oliveira LBA, de Oliveira RP, Oliveira C, et al. Cosmetic potential of a liotropic liquid crystal emulsion containing resveratrol. Cosmetics. 2017;4:54.
[2] Blanco-Fernández G, Blanco-Fernandez B, Fernández-Ferreiro A, et al. Lipidic lyotropic liquid crystals: insights on biomedical applications. Adv Colloid Interface Sci. 2023;313:102867.
[3] Rapalli VK, Waghule T, Hans N, et al. Insights of lyotropic liquid crystals in topical drug delivery for targeting various skin disorders. J Mol Liq. 2020;315:113771.
[4] Mezzenga R, Seddon JM, Drummond CJ, et al. Nature-inspired design and application of lipidic lyotropic liquid crystals. Adv Mater. 2019;31:1900818.
[5] Otón E, Otón JM, Caño-García M, et al. Rapid detection of pathogens using lyotropic liquid crystals. Opt Express. 2019;27:10098–10107.
[6] Santiago-Martoral L, Figueroa A, Nicolau E. Lyotropic liquid crystal-based membranes for water remediation: fabrication, characterization and performance evaluation. ACS Omega. 2020;5:17940–17946.
[7] Barauskas J, Nylander T. Lyotropic liquid crystals as delivery vehicles for food ingredients, in delivery and controlled release of bioactives in foods and nutraceuticals. Woodhead Publishing Series in Food Science. Technology and Nutrition. Chapt 4; 2008. 107–131.
[8] Kim YK, Senyuk B, Shin ST, et al. Surface alignment, anchoring transitions, optical properties, and topological defects in the thermotropic nematic phase of organo-siloxane tetrapodes. Soft Matter. 2014;10:500–509.

[9] Kim YK, Cukrov G, Vita F, et al. Search for microscopic and macroscopic biaxiality in the cybotactic nematic phase of new oxadiazole bent-core mesogens. Phys Rev E. 2016;93:062701.
[10] Nasrin L, Kabir E, Rahman M. External magnetic field-dependent tricritical points of uniaxial-to-biaxial nematic transition. Phase Trans. 2016;89:193–201.
[11] Yu LJ, Saupe A. Observation of a biaxial nematic phase in potassium laurate/1-decanol/water mixtures. Phys Rev Lett. 1980;45:1000–1003.
[12] Bartolino R, Chiaranza T, Meuti M, et al. Uniaxial and biaxial lyotropic nematic liquid crystals. Phys Rev A. 1982;26:1116–1119.
[13] Akpinar E, Guner E, Demir-Ordu O, et al. Effect of head-group size of some tetradecylalkylammonium bromide surfactants on obtaining the lyotropic biaxial nematic phase. Eur Phys J E. 2019;42(4):44.
[14] Freiser MJ. Ordered states of a nematic liquid. Phys Rev Lett. 1970;24:1041–1043.
[15] Alben R. Liquid crystal phase transitions in mixtures of rodlike and platelike molecules. J Chem Phys. 1973;59:4299–4304.
[16] Tans S, Verschueren A, Dekker C. Room-temperature transistor based on a single carbon nanotube. Nature. 1998;393:49–52.
[17] Baughman RH, Zakhidov AA, de Heer WA. Carbon nanotubes-the route toward applications. Science. 2020;297:787–792.
[18] de Heer WA, Châtelain A, Ugarte D. A carbon nanotube field-emission electron source. Science. 1995;270:1179–1180.
[19] Collins PG, Avouris P. Nanotubes for electronics. Sci Am. 2000;283(6):62–69.
[20] Rao CNR, Satishkumar BC, Govindaraj A, et al. Nanotubes. ChemPhysChem. 2001;2:78–105.
[21] Thostenson ET, Ren ZF, Chou TW. Advances in the science and technology of carbon nanotubes and their composites: a review. Composites Sci Technol. 2001;61:1899–1912.
[22] Weiss V, Thiruvengadathan R, Regev O. Preparation and characterization of a carbon nanotube-lyotropic liquid crystal composite. Langmuir. 2006;22:854–856.
[23] Baughman RH, Cui C, Zakhidov AA, et al. Carbon nanotube actuators. Science. 1999;284:1340–1344.
[24] Wong S, Joselevich E, Woolley A, et al. Covalently functionalized nanotubes as nanometre- sized probes in chemistry and biology. Nature. 1998;394:52–55.
[25] Kong J, Franklin NR, Zhou C, et al. Nanotube molecular wires as chemical sensors. Science. 2000;287:622–625.
[26] Dierking I, Scalia G, Morales P, et al. Aligning and reorienting carbon nanotubes with nematic liquid crystals. Adv Mater. 2004;16:865–869.
[27] Akpinar E, Topcu G, Reis D, et al. Effect of the presence of the anionic azo dye Sunset Yellow in lyotropic mixtures on the uniaxial-to-biaxial nematic phase transitions. J Mol Liq. 2020;318:114010.
[28] Horowitz VR, Janowitz LA, Modic AL, et al. Aggregation behavior and chromonic liquid crystal properties of an anionic monoazo dye. Phys Rev E. 2005;72:041710.
[29] Park H, Kang S, Tortora L, et al. Self-assembly of lyotropic chromonic liquid crystal Sunset Yellow and effects of ionic additives. J Phys Chem B. 2008;112:16307–16319.
[30] Akpinar E, Reis D, Neto AMF. Lyotropic mixture made of potassium laurate/1 undecanol/K_2SO_4/water presenting high birefringences and large biaxial nematic phase domain: a laser conoscopy study. Eur Phys J E. 2012;35:50.
[31] Akpinar E, Reis D, Neto AMF. Anomalous behavior in the crossover between the negative and positive biaxial nematic mesophases in a lyotropic liquid crystal. ChemPhysChem. 2014;15(7):1463–1469.
[32] Akpinar E, Uygur N, Demir-Ordu O, et al. Effect of the surfactant head-group size dependence of the dye-surfactant interactions on the lyotropic uniaxial to biaxial nematic phase transitions. J Mol Liq. 2021;332:11584.
[33] Dawin UC, Lagerwall JPF, Giesselmann F. Electrolyte effects on the stability of nematic and lamellar lyotropic liquid crystal phases: colligative and ion-specific aspects. J Phys Chem B. 2009;113(33):11414–11420.
[34] Akpinar E, Otluoglu K, Turkmen M, et al. Effect of the presence of strong and weak electrolytes on the existence of uniaxial and biaxial nematic phases in lyotropic mixtures. Liq Cryst. 2016;43(11):1693–1708.
[35] Collins KD. Charge density-dependent strength of hydration and biological structure. Biophys J. 1997;72 (1):65–76.
[36] Marcus Y. Effect of ions on the structure of water: structure making and breaking. Chem Rev. 2009;109:1346–1370.
[37] Phillips AJ, Henderson JA, Jackson KL. Pyrans and their benzo derivatives: structure and reactivity. Comprehen Heterocyclic Chem III. 2008;7(7):337–418.
[38] Hepworth JD, Gabbutt CD, Heron B.. Pyrans and their benzo berivatives: structure. In Comprehensive heterocyclic chemistry II. Chapt 5.07. Pergamon, Elsevier Sci. Ltd. 1996. 301–062350.
[39] Prasad S, Tantillo D. Substituent effects on the basicity of patriscabrin A and lettucenin A: evolution favors the aromatic? ACS Omega. 2021;6(44):29685–29691.
[40] Ibanez ACS, Luk ME, Y Y. Cromoglycate mesogen forms isodesmic assemblies promoted by peptides and induces aggregation of a range of proteins. RSC Adv. 2018;8:29598–29606.

[41] Leontidis E. Hofmeister anion effects on surfactant self-assembly and the formation of mesoporous solids. Curr Opin Colloid Interface Sci. 2002;7:81–91.
[42] Wen J, Shen X, Shen H, et al. Hofmeister series and ionic effects of alkali metal ions on DNA conformation transition in normal and less polarised water solvent. Mol Phys. 2014;112:2707–2719.
[43] Umapathi R, Reddy PM, Rani A, et al. Influence of additives on thermoresponsive polymers in aqueous media: a case study of poly(Nisopropylacrylamide). Phys Chem Chem Phys. 2018;20:9717–9744.
[44] Neto AMF, Galerne Y, Levelut AM, et al. Pseudo-lamellar ordering in uniaxial and biaxial lyotropic nematics: a synchrotron X-ray diffraction experiment. J Phys Lett. 1985;46:499–505.
[45] Galerne Y, Neto AMF, Liebert L. Microscopical structure of the uniaxial and biaxial lyotropic nematics. J Chem Phys. 1987;87:1851–1856 .